Int. J. Electrochem. Sci., 17 **(2022)** Article Number: 220213, doi: 10.20964/2022.02.30

International Journal of
ELECTROCHEMICAL
SCIENCE
www.electrochemsci.org

An Instantaneous Corrosion Monitoring Technique based on Combining Modified Electrochemical Noise and Artificial Neural Network for Determination of Corrosion Type and 2014 Aluminium Alloy Corrosion Rate in NaCl and $Ce(NO_3)_3$ solutions

Qiangfei Hu[1], *Tao Zhang*[2,*], *Shaohua Chen*[1], *Kun Hu*[1], *Qing Yin*[3], *Fuhui Wang*[2]

[1]Anhui Province Engineering Laboratory of Advanced Building Materials, Anhui Jianzhu University, Hefei 230601, P. R. China
[2] Corrosion and Protection Division, Shenyang National Laboratory for Materials Science, Northeastern University, Shenyang 110819, P. R. China
[3] Harbin Engineering University, Harbin 150001, P. R. China
[*]E-mail: zhangtao@mail.neu.edu.cn

Received: 1 November 2021 / *Accepted:* 7 December 2021 / *Published:* 5 January 2022

Electrochemical emission spectroscopy (EES), an improved electrochemical noise measurement, was applied for monitoring corrosion rate of 2014 aluminium alloy in NaCl and $Ce(NO_3)_3$, and corrosion type was analysed by wavelet transform and artificial neural network. Reliability of EES was verified by monitoring corrosion of 2014 aluminium alloy in the passivation, pitting and inhibition systems, because the results from EES, linear polarization resistance technique and morphology observation were in good agreement. In order to process data obtained by EES, artificial neural network was introduced to build the relationship between wavelet results and corrosion types, and results of confusion matrix and receiver operating characteristic curve demonstrated that artificial neural network is an excellent method for intelligent recognition for corrosion type.

Keywords: electrochemical noise; corrosion monitoring; corrosion rate; corrosion type; artificial neural network

1. INTRODUCTION

Metal corrosion assessment is of great importance from laboratory research to industrial monitoring [1]. Metal corrosion monitoring techniques mainly contain mechanical techniques (gravity method etc. al), physical techniques (sound waves detection etc. al) and electrochemical techniques. Electrochemical techniques, including Tafel extrapolation technique, linear polarization resistance

(LPR) test technique, electrochemical impedance spectroscopy (EIS) technique, and electrochemical noise (EN) technique, have advantages of easy monitoring corrosion rate and corrosion type [2, 3], so they are applied widely. In Tafel extrapolation technique the polarization curves are extrapolated from Tafel regions of either anodic or cathodic or both, and a cross-over point is determined at corrosion potential, where corrosion current density (i_{corr}) is easily available from current density axis [4]. So, it can obtain synchronously i_{corr} and Tafel parameters from this method. However, electrode polarization far from corrosion potential [5, 6] can alter specimen surface conditions and distort the results. Therefore, it is a destructive method and difficult to apply in the field of corrosion monitoring. From linear polarization resistance test technique, polarization resistance, R_p, can be calculated as the relationship $R_p = (\partial E/\partial I)$ when potential equals to corrosion potential, and based on Stern-Geary relationship ($i_{corr} = B/R_p$) corrosion current density can be obtained, where B can be calculated by the anodic and cathodic Tafel slopes [7]. It almost overcomes the destructive shortcomings because only a small region near free corrosion potential is investigated, and it is time-saving [8]. It can be used for online corrosion rate monitoring. But for conversion of polarization resistance to corrosion current density, Tafel parameter must be known beforehand, which provides little or no information to corrosion type. EIS is a method that usually applies a small AC signal (generally a sine wave with small potential amplitude) to a wide frequency range at a lot of discrete frequencies, and measures the AC response at each frequency. By analyzing EIS data, polarization resistance R_p can be obtained [9, 10], but it is hard to interpret EIS data. In addition, the full impedance is also time-consuming, which is a critical weak point in real-time corrosion monitoring application. The electrochemical techniques have damage to metal surface in different degrees, which is different from the freely corroding state in a known system.

In recent years, electrochemical noise technique is applied to corrosion monitoring [11-16]. It has three advantages: firstly, it overcomes the destructive nature of other techniques, where no external current or potential signal is necessary; secondly, it is time saving, by which corrosion rate can be determined even in 256 s; thirdly, it can recognize corrosion type of a corrosion system without additional disturbance by using the natural potential and current signal fluctuations [11-14]. Two equivalent electrodes are employed to determine corrosion rate in conventional EN technique, because noise resistance has a random and statistical nature, and there is an empirical relationship between polarization resistance and noise resistance [17-19]. However, it is extremely unrealistic to prepare two completely equivalent electrodes under field test conditions. In order to overcome this drawback, electrochemical emission spectroscopy (EES), an improved EN technique, is developed, where one work electrode is the monitored specimen, and the other one is replaced by a platinum wire electrode, providing a simple way to indicate localized corrosion. It has a great potential in industrial corrosion monitoring [11].

Because a large amount of data is obtained from EN monitoring, it is impractical to process these data manually. Artificial neural network (ANN) is a technique to deal with the problem. ANN can simulate human nervous system to learn and has been applied to solve problems of corrosion field [20-22]. Its greatest strong point is that the clear mathematical relationship between research factors and objectives is not required to be known; ANN learns and identifies patterns in factors and objective variables from experimental sample data without presuming their properties and relationships in advance [23-25]. In order to reduce the error between the predicted value and the observation value, the

connection weight between neurons is gradually adjusted and finally determined. Recently, ANN is introduced into corrosion field gradually. Birbilis [22] develops an ANN model for predicting corrosion rate of magnesium-rare earth alloys. Cavanaugh [26] applies ANN as a powerful tool to model maximum pit dimensions effectively, revealing that in most environment, pit growth rule followed $t^{1/3}$ kinetics. Kamrunnahar [20] used it to learn the basic law of the relationship between alloy element content, environmental factors and corrosion rate, so as to classify and prioritize some parameters, and understand the influence of the interaction between factors on corrosion. Sosa [27] firstly uses grey correlation analysis to study effect of many factors on external corrosion rate of oil and gas pipelines in soil, including soil physical and chemical properties, service length and coating performance; secondly, the influence weight of each factor is determined; lastly, by ANN the damage prediction model between pitting depth and external corrosion influencing factors is built. Hu [28] establishes the model between temperature, oxygen content, hydrostatic pressure and corrosion current density of a high strength steel in deep sea environment by using artificial neural network, and predicts the polarization curve of the material under different conditions. Lee [29] proposes an artificial neural network model to correlate the corrosion rate of 3C steel with seawater environmental factors. The prediction with the unobserved experimental data is in good agreement with the experimental values. In addition, the developed model is applied to simulate the comprehensive effects of environmental factors on corrosion rate. The effect of single factor on the corrosion rate is evaluated quantitatively.

In the present work, an instantaneous corrosion monitoring technique combining EES and ANN was developed to identify corrosion type and corrosion rate of 2014 aluminium alloy in NaCl and $Ce(NO_3)_3$ solutions. Firstly, the accuracy of corrosion rate monitoring by EES was verified by comparison with LPR technique results of 2014 aluminium alloy in different systems, such as passivation, pitting and inhibition system. Then, corrosion type was determined by wavelet analysis of EN data, which was associated with the micro corrosion morphology observation of the samples. Finally, artificial neural network was used to automatically recognize corrosion type from relative energy result of wavelet analysis.

2. BACKGROUND OF EN ANALYSIS

2.1 Wavelet analysis

Wavelet analysis is a typical analysis method for EN used in corrosion research. Supposing a time series x_p (p is a positive integer) in real space, wavelet method can be regarded as windowed Fourier analysis, which uses the basis composed of oscillatory functions with finite time span to represent time records x_p. The basis functions $\Psi_{q,m}$ and $\varphi_{q,m}$ originate from function Ψ and scaling function φ according to the follow transformation Eq.(1, 2):

$$\Psi_{q,m}(t) = 2^{-q/2}\Psi\left(\frac{t-2^q m}{2^q}\right). \quad (1)$$

$$\varphi_{q,m}(t) = 2^{-q/2}\varphi\left(\frac{t-2^q m}{2^q}\right). \quad (2)$$

where m is natural number from 1 to $P/2$, P is the time series number; q is natural number from 1 to Q, Q is a small positive integer which is determined primarily by P and the basis functions, both m and q belong to integers set. The scale parameter is 2^q, and the translation parameter is $2^q m$. The original time record $x(t)$ is reconstructed by linear superposition of basis functions $\Psi_{\mathrm{j,m}}$ and $\varphi_{\mathrm{j,m}}$ as Eq.(3):

$$x(t) = \sum_m s_{Q,m}\Psi_{Q,m}(t) + \sum_m d_{Q,m}\varphi_{Q,m}(t) + \sum_m d_{Q-1,m}\varphi_{Q-1,m}(t) + \cdots + \sum_m d_{1,m}\varphi_{1,m}(t). \quad (3)$$

where $s_{J,m}$, $d_{j,m}$, …, $d_{1,m}$ before basis functions are the corresponding coefficients. According to the algorithm of Eq. (3), decomposition of the time series signal, $x = (x_1, \underline{x}_2, \ldots, x_P)$, can be completed by a low and high frequency set, corresponding to the information of overall signal trend, and the local fluctuations detail information [30], and all coefficients (s_Q, d_1, d_2, …, d_Q) containing general trend and details are obtained. A coefficient set (s_Q, d_1, d_2, …, d_Q) is defined as a crystal, encoding different information characteristic of the original signal. The whole signal decomposition were carried out by using wavedec function in Matlab. The so-called sym of the eighth order orthogonal function φ(t) was applied.

After obtaining the coefficients, the relative energy (E_q) of each crystal was calculated. It corresponds to the name of the crystal, which is called the energy distribution plot (EDP). The overall signal energy is calculated as follow:

$$E = \sum_{p=1}^{p} x_p^2,\ p = 1,\ 2,\ ...,\ P. \quad (4)$$

In order to evaluate the contribution of each crystal to the whole crystal, the crystal relative energy is defined as following two equations:

$$E_q^d = \frac{1}{E}\sum_{m=1}^{P/2^q} d_{q,m}^2,\ q = 1,\ 2,\ ...,\ Q. \quad (5)$$

$$E_Q^S = \frac{1}{E}\sum_{m=1}^{P/2^Q} s_{Q,m}^2. \quad (6)$$

For details readers can refer to the papers of our work group [30, 31]. In our study EDP (E_q^d and E_Q^S versus crystal) are used to character localized corrosion type [30, 31].

2.2 Artificial neural network

Artificial neural network is a computing system which is inspired by the biological neural networks. It is based on a collection of connected units or nodes called artificial neural, which models the neural in a biological brain [20, 22]. Actually, it can be regarded as a highly complex modeling tool building complex relationships between any number of inputs properties and output targets, or looking for patterns in a large amount of data. ANN has inherent advantage in analyzing and predicting the system behavior, which cannot be directly expressed by analytical equations. The backpropagation artificial neural network is one of the most commonly used artificial neural network. A gradient descent

algorithm is used to minimize the average squared error between the network's outputs and the target values. Considering a given training set $\{(x_1, t_1), \ldots, (x_k, t_k)\}$, it has k groups of experimental samples, which has p input characteristics and q output characteristic, and neuron connection weights are randomly selected. When the input x_i (i = 1, 2, 3, …, k) in the training data set is transferred to the network, an output x_{oi} is obtained after calculation, which is generally different from the target t_i in the training data set. By gradually reducing the error function as Eq.(7) to the minimum value, the neuron weight and neural network are finally determined [20].

$$ferror = \frac{1}{2}\sum_{i=1}^{k}(x_{oi} - t_i)^2. \quad (7)$$

3. EXPERIMENT

3.1 Material and electrolyte

The research material is 2014 aluminum alloy (abbreviated as 2014AA) hot rolled plate, and its composition is displayed in Table 1. The samples processed by wire cutting were roughly ground to 240 grit-finish, degreased and dried, and then encapsulated in epoxy resin with 25 mm × 20 mm surface exposed for testing. All specimens were wet ground to 2000 grit-finish, washed with distilled water, degreased with alcohol and dried in hot air. The electrolyte solutions used were 0.6 mol/L NaCl, 0.03 mol/L $Ce(NO_3)_3$, and 0.6 mol/L NaCl + 0.03 mol/L $Ce(NO_3)_3$, which corresponded to pitting, passivation process and corrosion inhibition system.

Table 1. Composition of 2014 aluminium alloy (wt.%)

Si	Fe	Cu	Mn	Mg	Cr	Ni	Zn	Ti	Zr	Al
0.92	0.5	4.67	0.78	0.64	0.017	0.029	0.082	0.022	0.003	balance

3.2 Preparation of EES corrosion probe

Firstly, both the Ag/AgCl solid reference electrode and the 50 μm diameter platinum wire were embedded together in the epoxy resin as an EES probe. The structure is shown in Fig. 1. Secondly, the EES probe was wet ground to 2000 grit, washed with distilled water, degreased with alcohol and dried in hot air. Thirdly, the EES probe was activated in 0.15 mol/L dilute hydrochloric acid for a week.

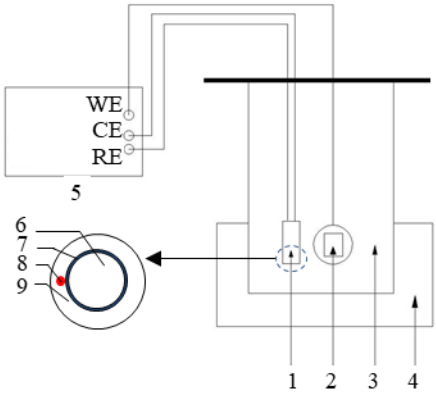

Figure 1. Diagram of the experimental device: (1) EES probe, (2) work electrode, (3) solution, (4) a constant temperature water bath, (5) electrochemical workstation, (6) Ag/AgCl solid reference electrode, (7) polyethylene, (8) copper wire, (9) epoxy resin

3.3 Electrochemical measurement

The classical three electrode system was used for linear polarization test. Platinum wire is used as the counter electrode and silver chloride electrode is applied as the reference electrode. In order to reach a relatively stable open circuit potential (OCP), the specimen was immersed for 15 min prior to the polarization test. The scanning rate of linear polarization test is 0.333 mV/s from -20 mV_{OCP} to 20 mV_{OCP}, once every 30 minutes during 3 hours immersion period.

Electrochemical noise tests were carried out by EES probe. Each group of electrochemical noise test has 2048 data points, and the sampling frequency is 5 Hz. The EN data soaked for 3 hours were collected, then it was analyzed in time domain and frequency domain, respectively. In the time domain, the noise resistance (R_n), which is conceptualized as the ratio of the standard deviation of potential noise to the standard deviation of current noise, is one of the most important parameters in statistical analysis, and it is be bound up with the polarization resistance (R_p). The reciprocal of noise resistance $1/R_n$ or polarization resistance $1/R_p$ is positively correlated to corrosion rate according to Stern-Geary relationship [32]. In addition, in the frequency domain, fast wavelet transform is applied to EN data analysis, and sym8 wavelet was used. In addition, the direct current trend is eliminated by 5th order polynomial fitting before EN analysis [30, 33].

Linear polarization test and EES experiments temperature was 25 ± 2^oC, and they were repeated at least three times for accuracy and reproducibility. In order to study accuracy of corrosion monitoring probe of EES, the results of R_n in different solutions were obtained from EES data, which associated with the polarization resistance R_p. The test solution compositions were displayed in Table 2. Corrosion types described were determined by micro corrosion morphology observation on the sample surface, and combining with the behavior of these corrosion systems and the interpretation of EES data by early researchers [34, 35].

Table 2. Concentration of solutions used to simulate different corrosion types [35]

Corrosion types	Solutions
Passivation	$Ce(NO_3)_3$ (0.06 mol/L)
Pitting	NaCl (0.6 mol/L)
Inhibition	NaCl (0.6 mol/L) + $Ce(NO_3)_3$ (0.03 mol/L)

3.4 ANN topology

The ANN topology shown in Fig. 2 is as follows: eight inputs, one hidden layer with 10 neurons, and three outputs, whose transfer functions are both tangential modulating functions (*tansig*). The inputs are relative energies E^d_j (i = 1, 2, …, 8) of current electrochemical noise signal by wavelet analysis, and outputs are corrosion types in different solutions. Intelligent recognition was applied by Matlab toolbox-nprtool, which has an ANN nature. In this pattern recognition, three different output classes representing corrosion types were coded as matrixes: passivation - type 1 - [0 0 1], pitting - type 2 - [0 1 0] and inhibition - type 3 - [1 0 0]. The optimization algorithm was the widely used Levenberg-Marquardt algorithm and error minimization tolerance value equaled 1%. A randomly selected 122 (75%) datasets and 16 (10%) datasets were employed for training and validation of the neural network, and the rest 24 datasets (15%) were applied to test. All the 162 datasets without normalized processing are shown in Appendix 1.

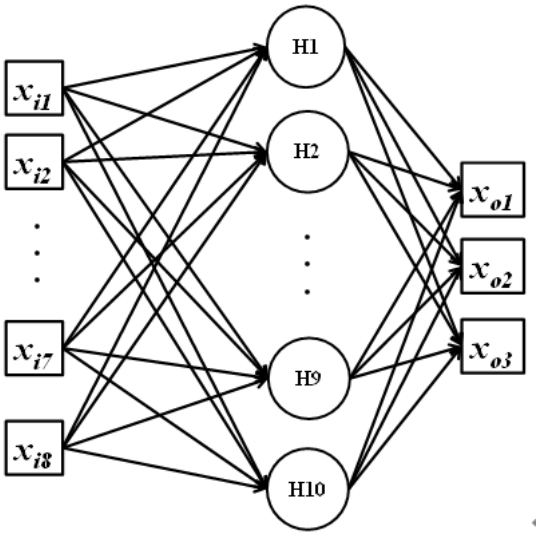

Figure 2. ANN topological structure used for intelligent recognition, which was composed of 8 inputs, a hidden layer with 10 nodes, and 3 outputs

4. RESULTS AND DISCUSSION

4.1 Reliability of corrosion rate monitoring by EES

During the immersion period, some typical transients electrochemical noise after DC trend removal of 2014AA in $Ce(NO_3)_3$, NaCl, and $Ce(NO_3)_3$ +NaCl solutions are recorded in Fig. 3-5, respectively. From Fig. 3a, during the immersion period shorter than 500 s, the same trend was depicted in both potential and current signals. Based on Butler-Volmer relationship in electrochemical theory, the experiment result demonstrated that 2014AA surface underwent anodic dissolution 2014AA [30]. During this period from 3600 s to 4100 s in Fig. 3b, it exists a relationship between potential and current noise that a positive potential noise matched a negative current noise shift, or a negative potential noise responded a positive current noise shift, which indicated that pitting corrosion occurred on 2014AA alloy surface. The trend from 7200 s to 7700 s in Fig. 3c was the same with that in Fig. 3b. In Fig. 3d the transient was in accordance with that in Fig. 3a.

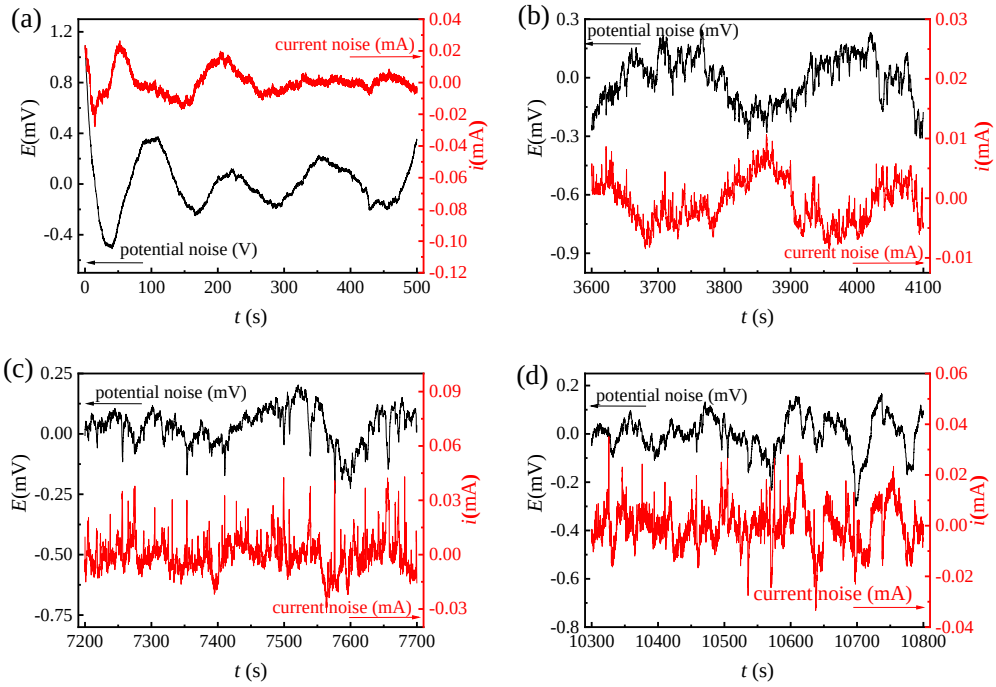

Figure 3. Typical electrochemical noise transients of 2014AA in $Ce(NO_3)_3$ solution during the different soaking time (a) from 0 to 500 s, (b) from 3600 to 4100 s, (c) from 7200 to 7700 s, (d) from 10300 to 10800 s

In Fig. 4a, during the first 500s, the potential and current noise signals are large, and then gradually decrease. During the immersion period from 3600 s to 4100 s in Fig. 4b, the opposite trend was depicted in the potential and current signal, demonstrating that 2014AA alloy surface undertook pitting corrosion. From 7200 s to 7700 s in Fig. 4c and from 10300 to 10800 s in Fig. 4d, the same trend with that in Fig. 4b was observed.

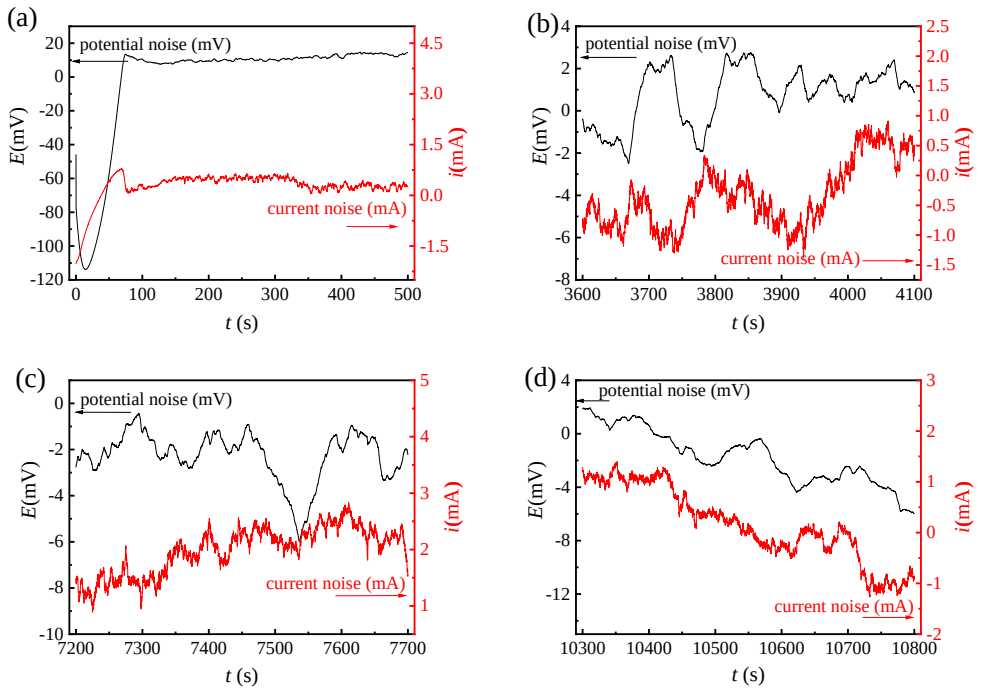

Figure 4. Typical electrochemical noise transients of 2014AA in NaCl solution during different soaking period (a) from 0 to 500 s, (b) from 3600 to 4100 s, (c) from 7200 to 7700 s, (d) from 10300 to 10800 s

In Fig. 5a, within less than 500 s, the increasing trend of current signal corresponded to the increasing trend of potential signal, and the decreasing trend of current signal corresponded to the decreasing trend of potential signal. In Fig. 5b, the same trend was seen in the potential and current signal before 3800s, however, in the second half of the time, potential and current signal was opposite. It can be referred that pitting corrosion occurred, and then it became activated anodic dissolution on 2014AA surface with pitting inhibited [30]. The trend of potential and current signals was consistent in Fig. 5c. In Fig. 5d, the potential signal trend was contrary to current signal trend in the early stage, but in the later stage potential and current signal trends were consistent. It can be seen that corrosion mechanism changed. From Fig. 5a-d it can be judged that the corrosion mechanism changed alternately.

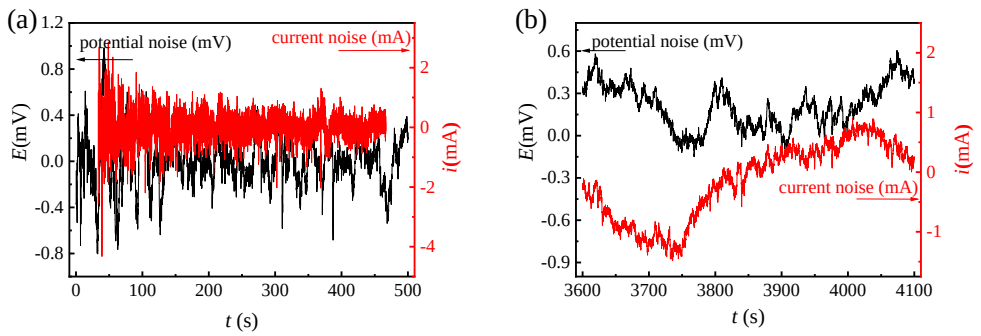

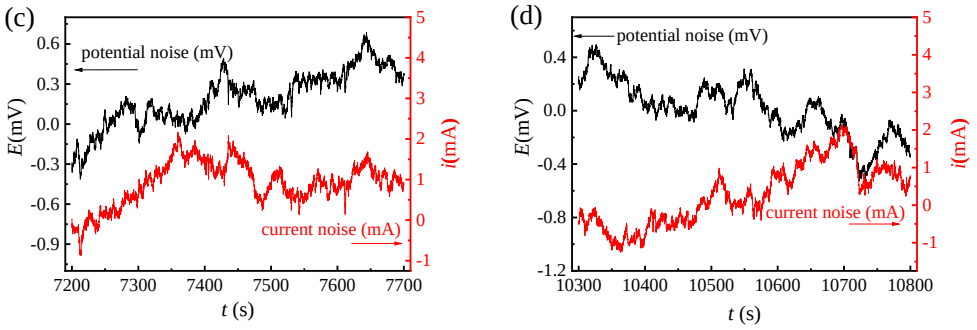

Figure 5. Typical electrochemical noise transients of 2014AA in $Ce(NO_3)_3$ + NaCl solution during the soaking time (a) from 0 to 500 s, (b) from 3600 to 4100 s, (c) from 7200 to 7700 s, (d) from 10300 to 10800 s

Fig. 6 records linear polarization results of 2014AA in different solutions, and slopes of these curves are R_p. Corrosion rate can be computed as $B/R_{p\ 0}$ for LPR technique and B/R_n [31] for EES technique, respectively. When corrosion type is pitting or inhibition, B is equal to 26 mV, and when corrosion type is passivation, B = 52 mV [36]. Fig. 7 shows corrosion rates exposed in $Ce(NO_3)_3$, NaCl, and $Ce(NO_3)_3$ +NaCl solutions varying with time. For different solutions corrosion rates obtained by LPR technique and EES technique were nearly the same. Fig. 7a depicts that $1/R_n$ and $1/R_p$ in $Ce(NO_3)_3$ solution was low and decreased gradually from about 1.78 $\mu A \cdot cm^{-2}$ to 0.9 $\mu A \cdot cm^{-2}$ with the immersion time. In NaCl solution, the value of corrosion rate was larger than that in $Ce(NO_3)_3$ solution, which was between 1.33 $\mu A \cdot cm^{-2}$ to 9.9 $\mu A \cdot cm^{-2}$ keeping at a high level shown in Fig. 7b. Fig. 7c demonstrates that in $Ce(NO_3)_3$ +NaCl solution corrosion rate of 2014AA reached a stable value 6.5 $\mu A \cdot cm^{-2}$. In three solutions, there were scatter, however, the shifts of i_{corr} by LPR technique and EES technique were consistent, which indicated that corrosion rate monitoring by EES in passivation, pitting and inhibition systems was practicable.

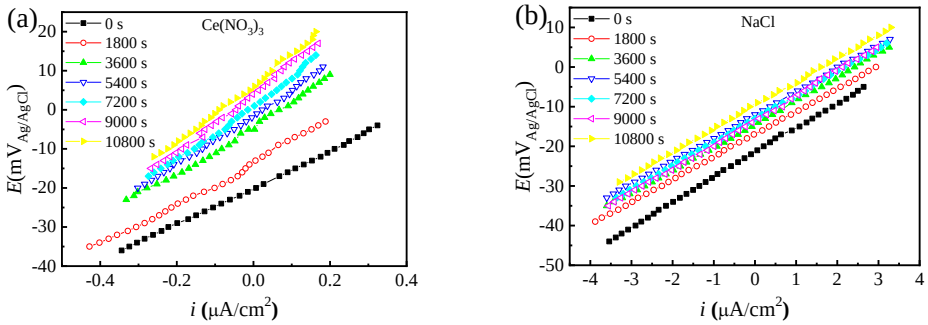

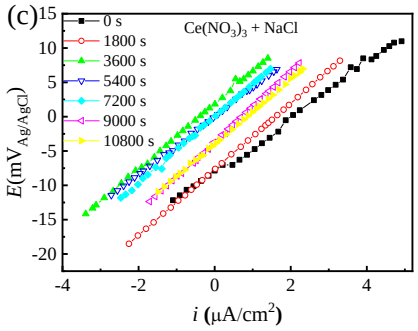

Figure 6. Linear polarization curves of 2014AA in (a) $Ce(NO_3)_3$, (b) NaCl, (c) $Ce(NO_3)_3$ +NaCl solution during the different immersion period

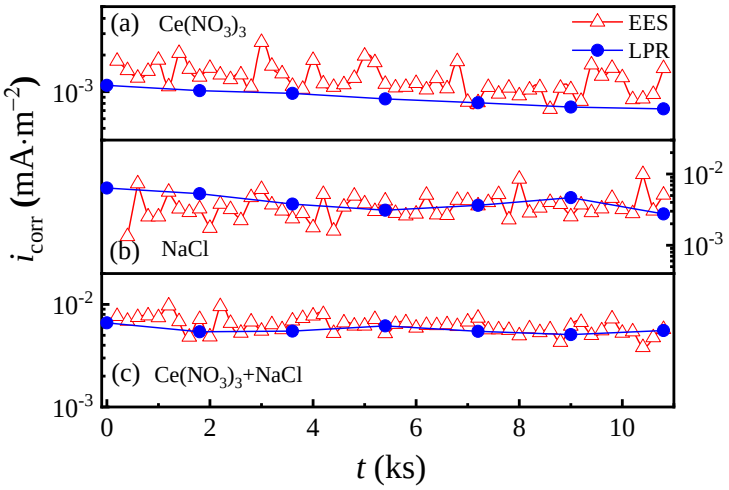

Figure 7. Corrosion rates of 2014AA by EES and LPR technique varying with immersion time in (a) $Ce(NO_3)_3$, (b) NaCl, (c) $Ce(NO_3)_3$ +NaCl solution

4.2 Reliability of corrosion type monitoring by EES

According to the literature [31], it is known that fast process responds to short time, and low process responds to short time long time. According to the time length of crystal *d*, it is arranged in descending order as follows: $d_8 > d_7 > \cdots > d_2 > d_1$. It can be known that corrosion nucleation process always occurs before growth process, and is much faster than diffusion and dissolution processes [30, 31].

The EDP diagram in a single time interval is a curve. If all EDP diagrams in multiple time periods are drawn together and smoothed by interpolation, the two-dimensional EDP (abbreviated as EDPs) containing EDPs of different time in the whole immersion period can be obtained. In Fig. 8a, it depicts the EDPs in correspondence with the current noise in $Ce(NO_3)_3$ solution during the immersion time displayed in Fig. 3. Consequently, relative energy of corrosion process mainly accumulated in crystals d_1-d_3, and d_7-d_8, respectively. From the domination in d_2 and d_8 crystal, it manifested that it mainly undertook nucleation/metastable pitting during continuous corrosion process. According to the micro

corrosion morphology result in Fig. 8b, 2014AA specimens indeed suffered from metastable pitting corrosion, and the pitting cavities with approximately 1-2 μm size scattered over the 2014AA specimen surface, which was in good agreement with the result of wavelet analysis.

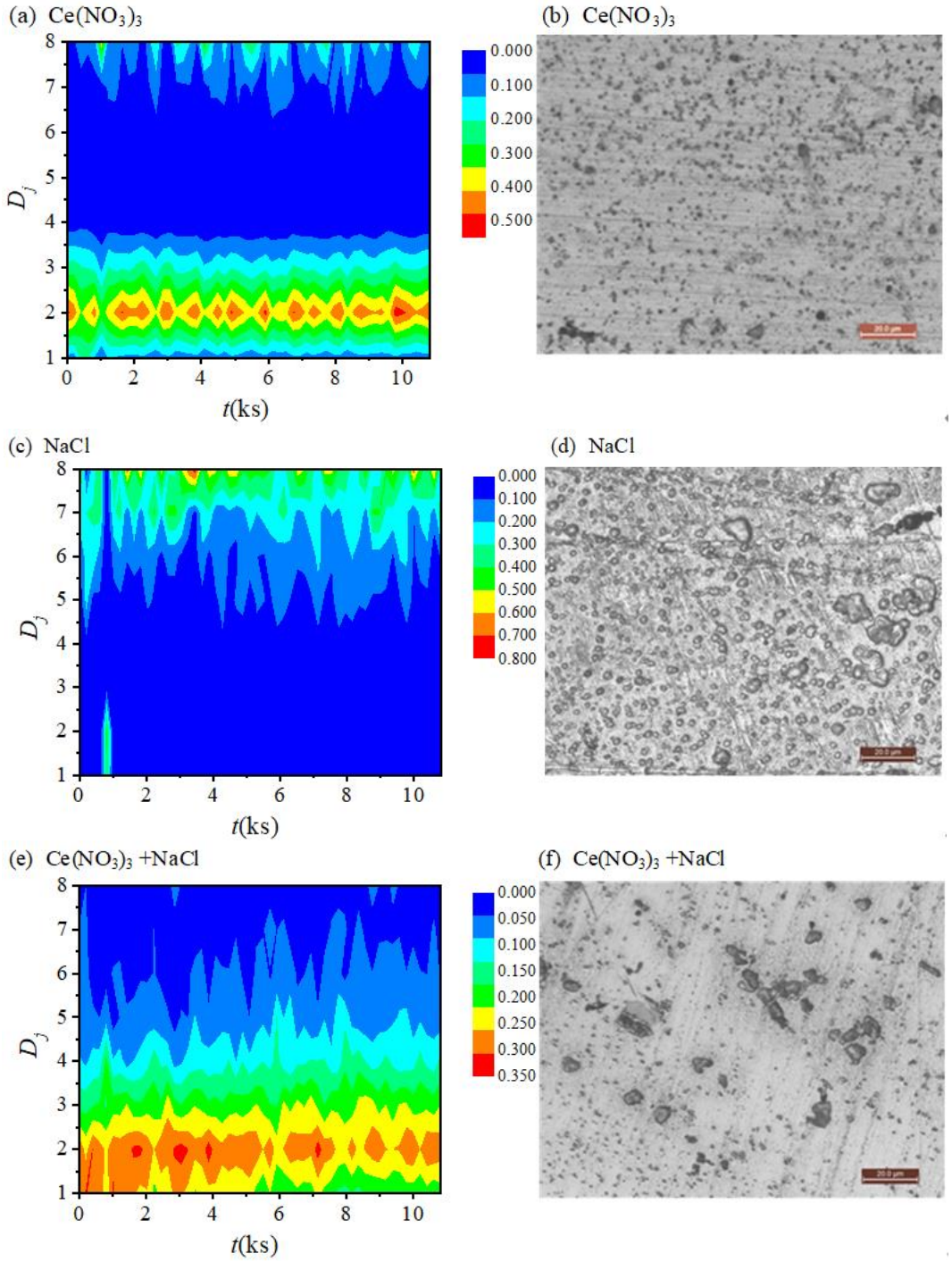

Figure 8. The EDPs and micro corrosion morphology of 2014AA after 10,800 s immersion in (a, b) $Ce(NO_3)_3$, (c, d) NaCl and (e, f) $Ce(NO_3)_3$ +NaCl solution

Fig. 8c shows EDPs during immersion period in accordance with the current noise in NaCl solution shown in Fig. 4. The relative energy distribution shows different characteristics. In the corrosion process, relative energy mainly concentrated in d_6 - d_8 crystals, and from d_6 to d_8 it increased gradually. Due to the details of the wavelet analysis of high frequency and low frequency corresponding to fast and slow corrosion process, respectively, it was inferred that from crystal d_6 2014AA underwent pitting corrosion, and from crystal d_8 diffusion process prevailed corrosion process. The results of corrosion morphology observation (in Fig. 8d) indicated that many pits with different sizes were observed on the sample surface, some of which were 4-5 μm. Results of wavelet analysis and corrosion morphology were in consistent with each other.

Fig. 8e presents the EDPs in correspondence with the current noise in $Ce(NO_3)_3$ + NaCl solution shown in Fig. 5. Relative energy accumulated in d_1-d_3 crystals. Moreover, energy decreased gradually from d_1 to d_8. Compared to EDPs of wavelet analysis in $Ce(NO_3)_3$ solution the relative energy in d_1 and d_2 crystals still remained high; however, the relative energy of large scale decreased, suggesting that diffusion and pitting growth may be inhibited. Generally, relative energy distribution accumulated at shorter time crystals for the solution with Ce^{3+} than that without the inhibitor. Compared with the results of 2014AA in NaCl solution, the relative energy maximum changed from large scales (d_7-d_8) to small scales (d_1-d_4). This suggested that once pitting initiation occurs at the beginning of corrosion, the pitting development will be inhibited by Ce^{3+} anions. This suggested that once a first event initiated during the corrosion process, the development of the pit was inhibited by the Ce^{3+} anion, which was similar with Aballe's result [37]. So, 2014AA in $Ce(NO_3)_3$ + NaCl solution mainly suffered from pitting nucleation and metastable pitting. The corrosion morphology of 2014AA in $Ce(NO_3)_3$ + NaCl solution revealed that the pit cavities with various sizes on the surface were observed in Fig. 8f. It should be noted that both the pitting size and pitting density were higher than that in $Ce(NO_3)_3$ solution, meanwhile, were lower than that in NaCl solution. This was attributed to the inhibition effect of Ce^{3+} anion [37]. In brief, according to the results in passivation, pitting and inhibition systems, it can be concluded that the determination of corrosion type based on wavelet analysis were reliable and accurate.

4.3 Intelligent recognition of corrosion type by ANN

A large amount of EDPs can be collected as training data of ANN, and an ANN model can be used to recognize corrosion type in different solutions. There are two indexes for evaluating the network, confusion matrix and receiver operating characteristic (ROC) [38]. In Fig. 9 it displays the confusion matrices for training, testing, and validation dataset, as well as the combination of the three datasets.

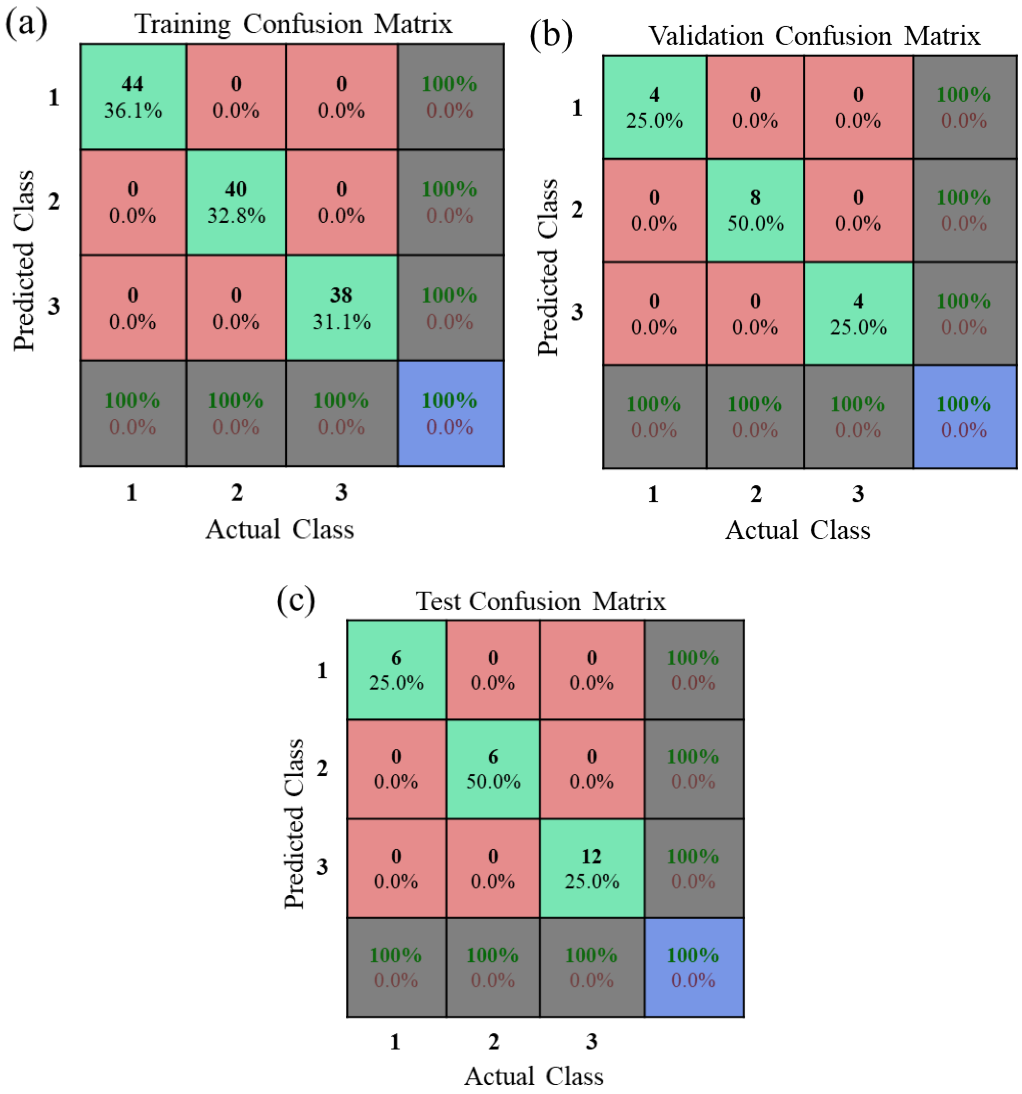

Figure 9. Confusion matrixes of ANN intelligent recognition of corrosion type for training, validation and test datasets: (a) training, (b) validation, (c) test c

From the result of the large number of correct responses in the green box and a small number of error responses in the red box, it can be seen that the network outputs were accurate. The blue box in the lower right corner shows high overall accuracy. In the training confusion matrix, horizontal coordinate and vertical coordinate represent actual corrosion type and predicted corrosion type by ANN, respectively. For example, in this confusion matrix at the upper left corner, all samples for actual 44 corrosion type 1 (36.1% in proportion) were correctly classified as corrosion type 1, and in the first line of the second column corrosion type 2 were incorrectly marked as corrosion type 1. All correct guesses are at the diagonal of the table, so it is ready to check the errors in the table because they are outside the diagonal. At the lower right corner, it represents the recognition rate of all the corrosion type. In the training datasets corrosion type has a 100% recognition rate. Similarly, in validation matrix and test matrix recognition ratio of all corrosion types reaches 100%, which manifests that intelligent recognition of corrosion type by ANN is reliable.

For statistics, receiver operating characteristic curve (ROC curve) is a graphical tool, which indicates the diagnostic ability of binary classifier system with recognition threshold varying, and it is generally used to estimate the classification performance. Considering a dichotomy problem, instances are divided into positive or negative classes. For a binary problem, there are four situations: if the instance is positive, and the model correctly or wrongly classifies it, the case is true positive (TP) or false negative (FP), respectively. Conversely, if the instance is negative, and the model is correctly or wrongly classified, it is defined as true negative (TN) or false negative (FN) [39]. According to previous definitions, two indicators can be determined: the true positive rate (TPR) defined by Eq. (8) and the false positive rate (FPR) calculated by Eq. (9) [39].

$$\mathrm{TPR} = \frac{\mathrm{TP}}{\mathrm{TP} + \mathrm{FN}}. \qquad (8)$$

$$\mathrm{FPR} = \frac{\mathrm{FP}}{\mathrm{FP} + \mathrm{TN}}. \qquad (9)$$

Fig. 10 presents the ROC graphic representing sensitivity against (1-specificity). Through the method, the best model is chosen according to the relative trade-off between TP and FP modes. Every point in the ROC graphical represents a classifier. In simple terms, ROC located near the upper left corner shows that the intelligent recognition by ANN provides a better classification performance. And the point (0, 1) in the upper left corner indicates a good classification.. Fig. 10a, Fig. 10b and Fig. 10c depict ROC curves of training, validation, and test datasets, respectively. Blue, green, and red lines curves overlap together, so it seems as only one red line. In Fig. 10, the ROC is closest to the upper left corner, so the ANN model with 10 hidden neurons exhibited very good classification characteristic. Both confusion matrix and ROC curves demonstrated that the ANN is an excellent method for intelligent recognition for corrosion type.

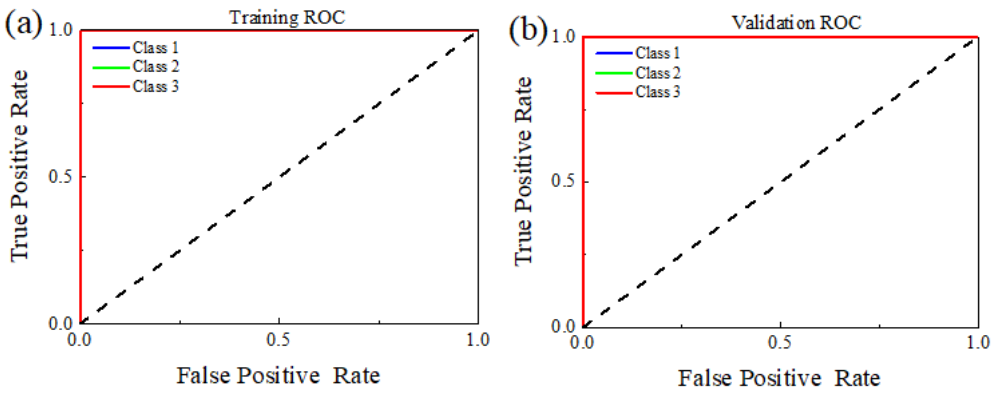

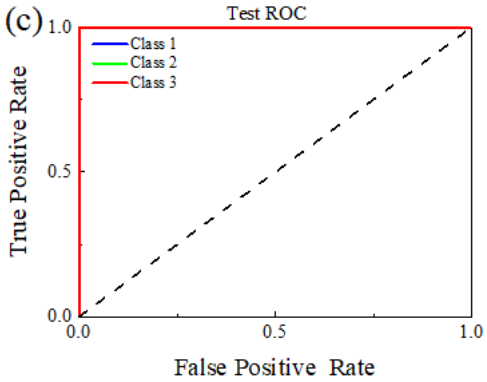

Figure 10. ROC curves of ANN intelligent recognition of corrosion type for (a) training, (b) validation and (c) test datasets

From the research EES with analysis via ANN exhibits some interesting and good perspectives for the field corrosion monitoring technique. Considering the large amount of field data, the application of relatively mature big data technology for ANN in corrosion monitoring in recent years is very promising, but there are some challenging issues to develop this kind of corrosion technique. Firstly, when many features (temperature, oxygen content, ions concentration etc.) are involved, ANN training may be hard to meet the requirements, maybe we can select several main variables through principal component analysis to reduce the scale of model training data; secondly, there is no specific basis for the selection of artificial neural network structure, but mainly depends on the judgment of experience; thirdly, ANN prediction is a prediction method based on data processing, which lacks physical basis, it is better to establish a hybrid model combining with a deterministic model, improving prediction accuracy.

5. CONCLUSIONS

An instantaneous corrosion monitoring technique combining EES and ANN is developed in order to determine corrosion type and corrosion rate. The corrosion rates and corrosion type of 2014AA in three corrosion solutions were measured and automatically recognized by the method, which agrees with the results of the standard LPR technique and morphology observation. It was also illustrated that this technique provides a feasible method to monitor localized corrosion.

The EES developed from the EN technique. Of course, it inherits all strong points of the EN technique. And the data analysis method of EN technology is also available for EES technique. Moreover, ANN is useful for intelligent recognition of corrosion type by processing thousands of EES data. From the results of confusion matrix and ROC curves, the ANN trained is successful in prediction and recognition of corrosion type.

ACKNOWLEDGEMENTS
The authors wish to acknowledge the financial support of phD Start-up Fund of Anhui Jianzhu University (2019QDZ01), Director Fund of Anhui Province Engineering Laboratory of Advanced Building Materials (JZCL010ZZ), Natural Science Foundation of Anhui Province (2008085QE274),

Key Natural Science Research Project of Department of Education of Anhui Province (KJ2020A0475), and the National Program for Support of Top-notch Young Professionals.

APPENDIX 1

Datasets of relative energy in different crystals and corresponding corrosion type for ANN training, validation, and test.

Crystal 1	Crystal 2	Crystal 3	Crystal 4	Crystal 5	Crystal 6	Crystal 7	Crystal 8	Corrosion type
0.10807	0.50133	0.23358	0.02543	0.02812	0.027	0.02899	0.04749	1
0.10455	0.44746	0.24192	0.02584	0.03096	0.0308	0.05415	0.06432	1
0.21947	0.33966	0.2096	0.0476	0.0184	0.01826	0.04361	0.1034	1
0.22799	0.37864	0.20308	0.04245	0.02054	0.02375	0.01477	0.08878	1
0.12755	0.44845	0.19172	0.02097	0.02475	0.03042	0.03776	0.11838	1
0.07424	0.31203	0.12025	0.01662	0.02457	0.02277	0.03631	0.39321	1
0.14148	0.37383	0.21035	0.03012	0.02236	0.03762	0.0797	0.10453	1
0.13103	0.42429	0.18511	0.03504	0.02436	0.02502	0.09111	0.08403	1
0.11946	0.49046	0.19815	0.01555	0.03096	0.03004	0.04538	0.07001	1
0.11467	0.4411	0.18999	0.01795	0.02719	0.02344	0.04591	0.13975	1
0.11314	0.43522	0.21533	0.01523	0.02865	0.0346	0.03763	0.12019	1
0.12803	0.47728	0.24837	0.0189	0.02574	0.03063	0.0431	0.02795	1
0.10563	0.42262	0.20717	0.01593	0.01627	0.04505	0.06648	0.12084	1
0.09157	0.3506	0.16756	0.0106	0.02315	0.05084	0.09388	0.2118	1
0.11489	0.47698	0.22455	0.0133	0.02309	0.04193	0.04567	0.0596	1
0.12066	0.46617	0.23612	0.02164	0.03369	0.04005	0.05258	0.02909	1
0.09337	0.36621	0.18269	0.01999	0.01883	0.04283	0.04918	0.2269	1
0.10419	0.39047	0.18078	0.01606	0.02624	0.02829	0.05688	0.19709	1
0.10632	0.44778	0.18625	0.0142	0.02076	0.02444	0.06523	0.13502	1
0.11564	0.46598	0.21702	0.0087	0.02669	0.03181	0.06723	0.06693	1
0.08235	0.35526	0.1457	0.0117	0.0209	0.02386	0.03678	0.32346	1
0.09707	0.39244	0.15676	0.01205	0.02714	0.0385	0.07794	0.1981	1
0.11657	0.47218	0.19396	0.01524	0.02679	0.03573	0.07959	0.05993	1
0.09603	0.39128	0.16883	0.01644	0.02403	0.02434	0.09744	0.1816	1
0.12168	0.49668	0.20131	0.0118	0.01815	0.0399	0.04403	0.06646	1
0.11373	0.44258	0.18956	0.01587	0.02168	0.05134	0.07903	0.08623	1
0.09596	0.40943	0.16519	0.00968	0.01359	0.03219	0.05438	0.21958	1
0.08986	0.36122	0.15178	0.01542	0.01782	0.01842	0.08132	0.26417	1
0.10543	0.41994	0.16876	0.01428	0.02309	0.03755	0.03697	0.19397	1
0.11691	0.50606	0.18883	0.01434	0.02105	0.02282	0.05956	0.07043	1

Crystal 1	Crystal 2	Crystal 3	Crystal 4	Crystal 5	Crystal 6	Crystal 7	Crystal 8	Corrosion type
0.09385	0.36401	0.15585	0.01101	0.01694	0.04385	0.12473	0.18975	1
0.10416	0.40349	0.17281	0.00996	0.01433	0.04852	0.09048	0.15625	1
0.09407	0.3951	0.16153	0.01343	0.01752	0.03417	0.0995	0.18469	1
0.11998	0.48862	0.22041	0.01793	0.01799	0.03707	0.0775	0.0205	1
0.12109	0.46896	0.20607	0.01044	0.01493	0.03034	0.03599	0.11217	1
0.10188	0.39651	0.19215	0.0108	0.01832	0.05868	0.06149	0.16017	1
0.11742	0.46328	0.19689	0.00821	0.01796	0.03126	0.04195	0.12302	1
0.10443	0.42192	0.17124	0.00982	0.01268	0.03498	0.05687	0.18805	1
0.09144	0.38115	0.1623	0.01304	0.01345	0.0336	0.05706	0.24794	1
0.11169	0.45385	0.19194	0.01579	0.01923	0.04348	0.10502	0.05901	1
0.10964	0.4827	0.20889	0.01228	0.02063	0.02609	0.03002	0.10974	1
0.08634	0.36129	0.16277	0.01193	0.01378	0.03832	0.12438	0.2012	1
0.10916	0.43123	0.21496	0.01119	0.02314	0.0431	0.06461	0.10261	1
0.11243	0.46625	0.21286	0.01859	0.01618	0.03944	0.06997	0.0643	1
0.11268	0.43444	0.17818	0.01494	0.02418	0.03749	0.06345	0.13464	1
0.10416	0.41816	0.17069	0.00753	0.02282	0.03305	0.07745	0.16615	1
0.10078	0.43447	0.19731	0.0185	0.01654	0.03206	0.07128	0.12906	1
0.11008	0.3834	0.20293	0.03884	0.01388	0.04562	0.0388	0.16646	1
0.12589	0.52045	0.24022	0.01468	0.01092	0.01189	0.04216	0.03379	1
0.10349	0.50079	0.2022	0.01344	0.01625	0.03456	0.05293	0.07635	1
0.10464	0.46832	0.19495	0.00683	0.00851	0.01739	0.04891	0.15045	1
0.09251	0.42181	0.19444	0.00715	0.00795	0.02231	0.0691	0.18472	1
0.10209	0.43977	0.20735	0.01858	0.01562	0.02503	0.07118	0.12037	1
0.10585	0.47823	0.22354	0.01385	0.01194	0.02197	0.06179	0.08284	1
0.22468	0.28232	0.2552	0.11659	0.04815	0.02631	0.01664	0.03012	2
0.27928	0.31348	0.19356	0.06924	0.02977	0.02449	0.03123	0.05895	2
0.26908	0.32568	0.17512	0.08167	0.04687	0.02931	0.03093	0.04135	2
0.25098	0.30759	0.19873	0.10588	0.04336	0.03802	0.043	0.01243	2
0.21326	0.27711	0.218	0.10793	0.09284	0.05396	0.02568	0.01122	2
0.22646	0.28391	0.20918	0.11391	0.05098	0.05826	0.03262	0.02468	2
0.24764	0.33151	0.18201	0.10407	0.05101	0.02865	0.03285	0.02227	2
0.25446	0.28894	0.19315	0.10807	0.06419	0.05276	0.03099	0.00745	2
0.23688	0.27662	0.17891	0.11224	0.07485	0.04693	0.02629	0.04728	2
0.22278	0.30307	0.1935	0.13351	0.06029	0.04736	0.0153	0.02419	2
0.22351	0.28699	0.20532	0.08612	0.06787	0.06372	0.03956	0.02692	2
0.22146	0.30004	0.18748	0.13301	0.06759	0.03833	0.03534	0.01676	2
0.24021	0.30591	0.20322	0.09706	0.0438	0.03105	0.03833	0.04042	2
0.20574	0.28885	0.22256	0.11347	0.07168	0.04949	0.04004	0.00819	2

Crystal 1	Crystal 2	Crystal 3	Crystal 4	Crystal 5	Crystal 6	Crystal 7	Crystal 8	Corrosion type
0.18471	0.26114	0.20775	0.13059	0.07952	0.06124	0.0402	0.03485	2
0.21963	0.29897	0.17716	0.12037	0.05625	0.0407	0.06877	0.01815	2
0.17786	0.24029	0.17311	0.1437	0.13283	0.05152	0.04288	0.03781	2
0.17784	0.26377	0.23064	0.11084	0.08701	0.05709	0.05167	0.02114	2
0.1798	0.30241	0.20386	0.09476	0.11654	0.06295	0.02999	0.0097	2
0.20984	0.27947	0.23267	0.12164	0.05249	0.03989	0.03734	0.02665	2
0.19431	0.28754	0.21544	0.12408	0.07823	0.04215	0.03322	0.02504	2
0.2014	0.27298	0.24309	0.13555	0.04488	0.05749	0.02961	0.01499	2
0.22933	0.32929	0.20953	0.132	0.05021	0.02682	0.01231	0.01052	2
0.20667	0.28856	0.17505	0.13432	0.08501	0.05372	0.0321	0.02458	2
0.19159	0.28232	0.2105	0.10331	0.05897	0.07314	0.04617	0.03401	2
0.16712	0.25158	0.21184	0.10296	0.11852	0.06137	0.06076	0.02585	2
0.15911	0.24492	0.19871	0.16849	0.12026	0.0277	0.05013	0.03068	2
0.17388	0.29074	0.19147	0.14019	0.07324	0.05982	0.02832	0.04234	2
0.1624	0.2497	0.23261	0.15701	0.06036	0.05463	0.06067	0.02262	2
0.18113	0.26715	0.24301	0.1316	0.05565	0.06221	0.03209	0.02714	2
0.17065	0.29144	0.23667	0.10705	0.06074	0.04461	0.0156	0.07325	2
0.17424	0.30172	0.19967	0.12054	0.06914	0.05152	0.04018	0.04299	2
0.19939	0.26337	0.22056	0.14434	0.06036	0.05868	0.03879	0.01451	2
0.17437	0.26254	0.19227	0.12385	0.08058	0.08007	0.02584	0.06047	2
0.1706	0.26694	0.22298	0.10129	0.09103	0.0697	0.03821	0.03926	2
0.19203	0.29894	0.22681	0.10587	0.09934	0.04568	0.01323	0.01811	2
0.19243	0.3077	0.19474	0.1141	0.06196	0.06104	0.03386	0.03415	2
0.18477	0.26196	0.20868	0.14707	0.0811	0.04506	0.02948	0.04188	2
0.20193	0.3002	0.21003	0.12055	0.06552	0.04328	0.03057	0.02791	2
0.17973	0.30364	0.1934	0.11044	0.06449	0.0716	0.04858	0.02811	2
0.19792	0.28814	0.2185	0.14063	0.06061	0.03934	0.03381	0.02105	2
0.01826	0.02504	0.02746	0.03554	0.04685	0.06171	0.05994	0.72536	3
0.01095	0.01705	0.01371	0.0219	0.03067	0.04276	0.12095	0.73905	3
0.01969	0.02894	0.02713	0.02842	0.04703	0.06072	0.15943	0.62791	3
0.01747	0.02271	0.01777	0.01596	0.0286	0.04279	0.05873	0.79476	3
0.01704	0.02277	0.01883	0.02066	0.0483	0.05957	0.20617	0.60638	3
0.02447	0.03047	0.02719	0.0263	0.03432	0.0574	0.0787	0.72189	3
0.027	0.03781	0.02742	0.02731	0.03251	0.0636	0.08339	0.69965	3
0.01916	0.02392	0.02059	0.03608	0.04608	0.04392	0.12294	0.68824	3
0.03724	0.04711	0.03942	0.03142	0.06044	0.06089	0.15244	0.56889	3
0.00879	0.01314	0.01558	0.01069	0.01334	0.03116	0.0442	0.86253	3
0.01312	0.01854	0.01724	0.01462	0.02537	0.04065	0.06943	0.80163	3

Crystal 1	Crystal 2	Crystal 3	Crystal 4	Crystal 5	Crystal 6	Crystal 7	Crystal 8	Corrosion type
0.042	0.051	0.04685	0.057	0.0655	0.0535	0.262	0.4225	3
0.0391	0.05427	0.04359	0.04915	0.0812	0.11068	0.10812	0.51282	3
0.02718	0.0343	0.03063	0.02602	0.02845	0.04296	0.1993	0.60915	3
0.04383	0.05765	0.04286	0.04505	0.05408	0.09796	0.24439	0.4148	3
0.02699	0.04286	0.02722	0.03545	0.10827	0.10489	0.38722	0.26654	3
0.02619	0.0346	0.03016	0.03206	0.05143	0.09175	0.1781	0.55873	3
0.02495	0.03083	0.03135	0.0342	0.05829	0.14197	0.1886	0.48964	3
0.02208	0.02778	0.0264	0.02949	0.05365	0.07472	0.17303	0.5927	3
0.02212	0.02615	0.02514	0.03715	0.04525	0.18464	0.42458	0.23575	3
0.03112	0.0412	0.0412	0.05468	0.08652	0.11124	0.22921	0.40449	3
0.02495	0.03495	0.02929	0.04045	0.05437	0.10744	0.07864	0.63107	3
0.01713	0.02211	0.01826	0.02231	0.03202	0.0657	0.11219	0.71074	3
0.02152	0.03188	0.02931	0.03753	0.07249	0.06452	0.57069	0.17275	3
0.02194	0.02926	0.02336	0.0247	0.04341	0.08705	0.09544	0.67626	3
0.00755	0.01113	0.00907	0.00911	0.01349	0.02821	0.14245	0.77925	3
0.00902	0.01268	0.01179	0.00792	0.01703	0.04227	0.13043	0.76932	3
0.01152	0.01741	0.01118	0.01168	0.02348	0.02923	0.0647	0.83067	3

References

1. L. Chen, D.M. Fu, and M.D. Chen, *J. Mater. Sci.*, 55 (2020)13398.
2. J.F. Chen, and W. Bogaerts, *Corrosion*, 52 (1996) 753.
3. Y. Hou, C. Aldrich, K. Lepkova, L.L. Machuca, and B. Kinsella, *Corros. Sci.*, 112 (2016) 63.
4. D.A. Fischer, I.T. Vargas, G.E. Pizarro, F. Armijo, and M. Walczak, *Electrochim. Acta*, 313 (2019) 457.
5. A.R. El-Sayed, H.S. Mohran, and H.M. Abd El-Lateef, *Metall. Mater. Trans. A*, 43A (2012) 619.
6. V.S. Shaldaev, A.N. Malofeeva, and A.D. Davydov, *Russ. J. Electrochem.*, 50 (2014) 994.
7. L.J. Chen, and R.K.L. Su, *Constr. Build. Mater.*, 15 (2021) 267.
8. R. Rodrigues, S. Gaboreau, J. Gance, I. Ignatiadis, and S. Betelu, *Constr. Build. Mater.*, 36 (2021) 269.
9. C. Thee, L. Hao, J.-H. Dong, X. Mu, and W. Ke, *Acta. Metall. Sin. (Engl. Lett.)*, 28 (2015) 261.
10. M. Guo, J. Tang, T. Gu, C. Peng, Q. Li, C. Pan, and Z. Wang, *Acta. Metall. Sin. (Engl. Lett.)*, 34 (2021) 555.
11. D.H. Xia, S. Song, Y. Behnamian, W. Hu, Y.F. Cheng, J.-L. Luo, and F. Huet, *J. Electrochem. Soc.*, (2020) 167.
12. D.-H. Xia, S. Song, Z. Qin, W. Hu, and Y. Behnamian, *J. Electrochem. Soc.*, (2019) 167.
13. C. Ma, Z. Wang, Y. Behnamian, Z. Gao, Z. Wu, Z. Qin, and D.-H. Xia, *Measurement*, 54 (2019) 138.
14. D.H. Xia, S.Z. Song, and Y. Behnamian, *Corros. Eng. Sci. Techn.*, 51 (2016) 527.
15. Z. Zhang, X. Li, Z. Zhao, P. Bai, B. Liu, J. Tan, and X. Wu, *J. Electroanal. Chem.*, (2020) 879.
16. C.I. Rocabruno-Valdes, R.F. Escobar-Jimenez, Y. Diaz-Blanco, J.F. Gomez-Aguilar, C.M. Astorga-Zaragoza, and J. Uruchurtu-Chavarin, *J. Electroanal. Chem.*, (2020) 878.

17. D.H. Xia, C. Ma, S. Song, and L. Xu, *J. Electrochem. Soc.*, 166 (2019) B1000.
18. J. Lv, Q. Yue, R. Ding, X. Wang, T. Gui, and X. Zhao, *Chemelectrochem*, 8 (2021) 337.
19. W.W. Cheng, S.Y. Luo, and Y. Chen, *Int. J. Electrochem. Sc.*, 14 (2019) 4254.
20. M. Kamrunnahar, and M. Urquidi-Macdonald, *Corros. Sci.*, 52 (2010) 669.
21. M. Kamrunnahar, and M. Urquidi-Macdonald, *Corros. Sci.*, 53 (2011) 961.
22. N. Birbilis, M. Cavanaugh, A. Sudholz, S.-M. Zhu, M. Easton, and M. Gibson, *Corros. Sci.*, 53 (2011) 168.
23. J. Kubisztal, M. Kubisztal, and G. Haneczok, *Mater. Corros.*, 71 (2020) 1842.
24. Q.F. Hu, Y.C. Liu, T. Zhang, S.J. Geng, and F.H. Wang, *J. Mater. Sci. Technol.*, 35 (2019) 168.
25. M.J. Jimenez-Come, M.D. Martin, V. Matres, and J.D.M. Balades, *Corros. Rev.*, 38 (2020) 339.
26. M.K. Cavanaugh, R.G. Buchheit, and N. Birbilis, *Corros. Sci.*, 52 (2010) 3070.
27. E. Sosa, A. V. Martinez, J. L. Alamilla, A. Contreras, L.M. Quej, and H. Liu, *Corros. Rev.*, 38 (2020) 433.
28. Q.F. Hu, Y.C. Liu, T. Zhang, S.J. Geng, and F.H. Wang, *J. Mater. Sci. Technol.*, 35 (2019) 168.
29. S. Lee, P.L. Narayana, W.S. Bang, B.B. Panigrahi, S.G. Lim, and N.S. Reddy, *J. Mater. Sci. Technol.*, 11 (2021) 681.
30. T. Zhang, Y. Shao, G. Meng, and F. Wang, *Electrochim. Acta*, 53 (2007) 561.
31. X. Liu, T. Zhang, Y. Shao, G. Meng, and F. Wang, *Corros. Sci.*, 52 (2010) 892.
32. M. Stern, and A.L. Geary, *J. Electrochem. Soc.*, 104 (1957) 56.
33. T. Zhang, Y. Cong, Y. Shao, G. Meng, and F. Wang, *J. Appl. Electrochem.*, 41 (2011) 289.
34. H.A.A. Al-Mazeedi, and R.A. Cottis, *Electrochim. Acta*, 49 (2004) 2787.
35. J.M. Sanchez-Amaya, R.A. Cottis, and F.J. Botana, *Corros. Sci.*, 47 (2005) 3280.
36. J. Wei, C.G. Wang, X. Wei, X. Mu, X.Y. He, J.H. Dong, and W. Ke, *Acta. Metall. Sin. (Engl. Lett.)*, 32 (2019) 900.
37. A. Aballe, M. Bethencourt, F.J. Botana, M. Marcos, and R.M. Osuna, *Electrochim. Acta*, 47 (2002) 1415.
38. T. Fawcett, *Pattern. Recogn. Lett.*, 27 (2006) 861.
39. M. Jesus Jimenez-Come, I.J. Turias, and J. Jesus Ruiz-Aguilar, *Corros. Rev.*, 34 (2016) 113.